


Stability and conductivity of cation- and anion-substituted  $\text{LiBH}_4$ -based solid-state electrolytes

Zhenpeng Yao,<sup>\*</sup> Soo Kim,<sup>†</sup> Kyle Michel,<sup>‡</sup> Yongsheng Zhang,<sup>§</sup> Muratahan Aykol,<sup>||</sup> and Chris Wolverton<sup>¶</sup>  
*Department of Materials Science and Engineering, Northwestern University, 2220 Campus Drive, Evanston, Illinois 60208, USA*

 (Received 18 March 2018; published 19 June 2018)

The high-temperature phase of  $\text{LiBH}_4$  (HT- $\text{LiBH}_4$ ) exhibits a promisingly high lithium ion conductivity but is unstable at room temperature. We use density functional theory (DFT) calculations to investigate the stabilization effect of halogen and alkali cation/anion substitutions on HT- $\text{LiBH}_4$  as well the underlying mechanism for the high lithium ion conductivity. We find that increasing the substituent concentration enhances the stabilization of HT- $\text{LiBH}_4$  (i.e., the DFT energy difference between the low- and high-temperature forms of substituted  $\text{LiBH}_4$  is reduced). Cation/anion substitution also leads to a higher Li defect (vacancy, interstitial, and Frenkel) formation energy, thereby reducing the Li defect (vacancy, interstitial, and Frenkel) concentrations. Using DFT migration barriers input into kinetic Monte Carlo simulations and the Materials INterface (MINT) framework, we calculate the room-temperature lithium ion conductivities for  $\text{Li}(\text{BH}_4)_{1-x}\text{I}_x$  ( $x = 0.25$  and  $0.5$ ) and  $\text{Li}_{1-y}\text{K}_y\text{BH}_4$  ( $y = 0.25$ ). Our calculations suggest that the lower I concentration leads to a higher lithium ion conductivity of  $5.7 \times 10^{-3}$  S/cm compared with that of  $\text{Li}(\text{BH}_4)_{0.5}\text{I}_{0.5}$  ( $4.2 \times 10^{-5}$  S/cm) because of the formation of more Li-related defects. Based on our findings, we suggest that the stabilization of HT- $\text{LiBH}_4$ -based lithium ion conductors can be controlled by carefully tuning the cation/anion substituent concentrations to maximize the lithium ionic conductivities of the specific system.

DOI: [10.1103/PhysRevMaterials.2.065402](https://doi.org/10.1103/PhysRevMaterials.2.065402)

## I. INTRODUCTION

Lithium-ion batteries (LIBs) have been prominent electrochemical energy storage systems over the past two decades, enabling the wireless evolution of portable electronic devices [1]. Since the commercialization of LIBs [2], only organic liquid electrolytes have been used in commercial systems. However, their use poses a significant safety concern for emerging applications such as electric vehicles and grid storage because of the high risk of leakage [3] and flammability [4]. In addition, dendritic lithium growth over extended cell cycling can lead to short circuits in LIBs when the organic liquid electrolyte is used [5]. Some cathode materials also have a tendency to dissolve in the electrolyte (e.g., Mn ions in  $\text{LiMn}_2\text{O}_4$  spinel cathodes), which can further impair the overall efficiency of LIBs [6]. To circumvent these issues, the replacement of organic liquid electrolytes with inorganic solid-state electrolytes (SSEs) is being actively pursued [7]. Various types of crystalline lithium

conducting SSE materials have been studied to date, including lithium nitrides [8], lithium hydrides [9–14], perovskite-type oxides [15], argyrodites [16], garnets [17], NASICON [18], LISICON [19], and  $\text{Li}_{10}\text{MP}_2\text{S}_{12}$  ( $M = \text{Si}, \text{Ge}, \text{Sn}$ ) [20,21]. Among these candidates, lithium borohydride ( $\text{LiBH}_4$ ) shows interesting potential for battery applications [22] because of its (i) fast lithium ion conductivity, (ii) low grain boundary resistance, (iii) negligible electronic conductivity, (iv) high electrochemical stability (up to  $\sim 5$  V versus  $\text{Li}/\text{Li}^+$ ), and (v) high chemical stability against decomposition in contact with lithium metal and/or graphite-based anode materials. Previously,  $\text{LiBH}_4$  has also been extensively studied as a potential candidate for hydrogen storage applications [23–25].

The low-temperature (LT) phase of  $\text{LiBH}_4$  (denoted as LT- $\text{LiBH}_4$  in this work) has an orthorhombic  $Pnma$  structure and undergoes a structural phase transition to the hexagonal  $P6_3mc$  phase above  $\sim 390$  K. The high-temperature (HT) phase of  $\text{LiBH}_4$  (denoted as HT- $\text{LiBH}_4$  in this work) exhibits high ionic conductivity on the order of  $10^{-3}$  S/cm [26] and is an electrical insulator with a large band gap of  $\sim 6$  eV [27], making it highly promising for use as a SSE in LIBs [28–30]. Previous studies have also shown that the incorporation of lithium halides ( $\text{LiX}$ , where  $X = \text{Cl}, \text{Br}, \text{I}$ ) into the  $\text{LiBH}_4$  structure can lead to the formation of a solid solution [i.e.,  $x\text{LiX}(1-x)\text{LiBH}_4$ ] over a wide range of concentrations, which can further reduce the LT- $\text{LiBH}_4$  to HT- $\text{LiBH}_4$  phase transition temperature (we refer to this phenomenon as the “stabilization” of HT- $\text{LiBH}_4$  in this work) [9,31–36]. The substitution of LiI into the  $\text{LiBH}_4$  structure not only provides a stabilizing effect but also results in a very high lithium ion conductivity [9,37–39]. Another effective strategy to reduce the phase transition temperature of  $\text{LiBH}_4$  involves substituting Li with other alkali elements such as Na and K [40,41]. However, the relationship between the lithium

<sup>\*</sup>Present address: Department of Chemistry and Chemical Biology, Harvard University, 12 Oxford Street, Cambridge, Massachusetts 02138, USA.

<sup>†</sup>Present address: Research Laboratory of Electronics, Massachusetts Institute of Technology, 77 Massachusetts Avenue, Cambridge, Massachusetts 02139, USA.

<sup>‡</sup>Present address: Citrine Informatics, Inc., 1741 Broadway #300, Redwood City, CA 94063, USA.

<sup>§</sup>Present address: Key Laboratory of Materials Physics, Institute of Solid State Physics, Chinese Academy of Sciences, Hefei 230031, China.

<sup>||</sup>Present address: Toyota Research Institute, 4440 El Camino Real, Palo Alto, CA 94022, USA.

<sup>¶</sup>Corresponding author: [c-wolverton@northwestern.edu](mailto:c-wolverton@northwestern.edu)

halide incorporation/alkali metal substitution and the reduction of the phase transition temperature is not well understood. Meanwhile, the energetic impact of the incorporations and substitutions on the lithium ion conductivities in the related systems need further clarification.

Density functional theory (DFT) calculations can help to predict new prototype compounds, generate phase diagrams, calculate electrochemical stability windows, induce defect formation energies, and determine ionic conductivities [42–60], which can all be used to facilitate the design and improvement of new lithium-ion conducting materials. In this work, we report on the stabilization effects (i.e., reduction of the energy difference between LT- and HT-LiBH<sub>4</sub>) achieved through elemental substitutions with alkali metals and halogens using standard DFT calculations. Additionally, we determined the defect concentrations and lithium ion conductivities using native defect formation energy calculations, with the combination of the nudged elastic band (NEB) method and kinetic Monte Carlo (KMC) simulations for the targeted systems. Finally, we analyzed the relations between the ionic conductivity and stabilization effects that are highly dependent on both the substituents and their concentrations in LiBH<sub>4</sub>-based lithium-ion conducting materials. Our calculations suggest that the relatively lower I concentration leads to a higher lithium ion conductivity of  $5.7 \times 10^{-3}$  S/cm compared with that of Li(BH<sub>4</sub>)<sub>0.5</sub>I<sub>0.5</sub> ( $4.2 \times 10^{-5}$  S/cm) because of the formation of more Li-related defects. Based on our findings, we suggest that the maximum stabilization and lithium ionic conductivities of a specific system can be achieved by carefully tuning the cation/anion substituent concentrations.

## II. METHODOLOGY

### Computational details and structure determination

All the total energies were obtained using DFT calculations within the Vienna *ab initio* simulation package (VASP) [61]. We used the PW91 [62] generalized gradient approximation (GGA) to the exchange-correlation energy with the projector augmented wave (PAW) [63] method and a plane-wave cutoff energy of 875 eV based on previous studies [25,64,65]. For the ion-substituted structures of LiBH<sub>4</sub>, we started with a supercell of HT *P6<sub>3</sub>mc* and LT *Pnma* phase structures of LiBH<sub>4</sub> containing 16 formula units (96 atoms). For the cation/anion-substituted LiBH<sub>4</sub>, we used ENUM [66] to generate all derivative configurations with various compositions and substituent concentrations [67]. After relaxation of all these structures within VASP, we chose the structure with the lowest DFT energy for further analysis. Defects were introduced in supercells of HT-LiBH<sub>4</sub>, Li(BH<sub>4</sub>)<sub>1-x</sub>I<sub>x</sub> ( $x = 0.25$  and  $0.5$ ), and Li<sub>1-y</sub>K<sub>y</sub>BH<sub>4</sub> ( $y = 0.25$ ) that contained 96, 80, and 96 atoms after a series of convergence tests, respectively. For all of these calculations, we used  $\Gamma$ -centered  $k$  meshes with a density of 8000  $k$  points per reciprocal atom. The atomic coordinates were relaxed until the total energy converged to within  $10^{-5}$  eV and the interatomic forces were below  $10^{-2}$  eV/Å. The defect formation energies and concentrations were calculated using Eqs. (S3)–(S10) (see Ref. [68]) considering all the geometrically different vacancy and interstitial sites [68]. Defect conductivity calculations were conducted using KMC simulations based on

the NEB [69,70] method and defect energetics [68]. The whole process is automated with the Materials INTERface (MINT) package [65,71,72].

### III. STABILIZATION OF HT-LIBH<sub>4</sub> BY HALOGEN AND ALKALI METAL SUBSTITUTION

We begin by evaluating the stabilization of the HT-LiBH<sub>4</sub> phase via various ionic substitutions with halogen (F, Cl, Br, and I) and alkali (Na, K) elements. We calculated the DFT energy differences ( $\Delta E$ ) between the HT- and LT-LiBH<sub>4</sub> phases:  $\Delta E = E_{\text{HT}} - E_{\text{LT}}$ , where  $E_{\text{HT}}$  and  $E_{\text{LT}}$  are the energies of partially substituted HT- and LT-LiBH<sub>4</sub> structures, respectively. Considering that the stabilization effects can further depend on the substituent concentration, we repeated the calculation for a series of concentrations:  $x, y = 0.125, 0.25$ , and  $0.50$  in  $x\text{LiX}(1-x)\text{LiBH}_4$  and  $y\text{ABH}_4(1-y)\text{LiBH}_4$ .

Both the anion (F, Cl, Br, I) and cation (Na, K) substitutions decreased the energy difference between the substituted HT- and LT-LiBH<sub>4</sub> phases, as observed in Fig. 1(a). In addition, a higher substituent concentration further reduced the energy difference (i.e., an enhanced stabilization effect). Therefore all substitutions tend to stabilize the HT-LiBH<sub>4</sub> phase while better stabilization is achieved with higher substitution concentration.

We also computed the DFT volumes (per formula unit) of the cation/anion-substituted HT-LiBH<sub>4</sub> structures, as shown in Fig. 1(b). We found that K<sup>+</sup> and I<sup>-</sup> ions with larger effective radii (K<sup>+</sup>: 1.51 Å, I<sup>-</sup>: 2.06 Å) [73] directly contributed to the increase of the cell volumes in the substituted LiBH<sub>4</sub> structures, whereas the substitutions of ions with smaller ionic radii (e.g., Br<sup>-</sup>: 1.82 Å and Cl<sup>-</sup>: 1.67 Å) [73] only had a limited effect on the final cell volume. Based on the variations among the predicted cell volumes in Fig. 1(b), we conclude that the size differences of the substituents exhibit limited influence on the stabilization effects [38].

In Fig. 1(c), we present the calculated mixing energies of HT-LiBH<sub>4</sub>, ABH<sub>4</sub> ( $A = \text{Na, K}$ ), and LiX ( $X = \text{F, Cl, Br, I}$ ) using equation S1-S2. Moderate-sized substituents (e.g., Br<sup>-</sup>: 1.82 Å, Cl<sup>-</sup>: 1.67 Å, Na<sup>+</sup>: 1.13 Å) [73] led to a lower mixing energy than those with large ionic radii (e.g., K<sup>+</sup>: 1.51 Å, I<sup>-</sup>: 2.06 Å) [73] or small ionic radii (e.g., F<sup>-</sup>: 1.33 Å) [73] in HT-LiBH<sub>4</sub>. All the mixing energies calculated in Fig. 1(c) were negative (except F<sup>-</sup>, slightly positive: +15 meV) as predicted for several of them in previous studies [74–76], which explains the strong tendency of mixing between HT-LiBH<sub>4</sub> and LiX ( $X = \text{Cl, Br, I}$ ) [34] or ABH<sub>4</sub> ( $A = \text{Na, K}$ ) [40] for the wide range of substituent concentrations. A negative mixing energy ( $E_{\text{mix}} < 0$ ) implies that there could be stable ordered compounds at 0 K and a positive mixing energy ( $E_{\text{mix}} > 0$ ) implies the tendency of phase separation. Small positive or negative mixing energies ( $-30 \text{ meV/atom} < E_{\text{mix}} < 30 \text{ meV/atom}$ ) could be overcome by entropy, and hence results in a stable solid solution at elevated temperatures. Relatively large negative mixing energies are observed for many compositions as shown in Fig. 1(c), which indicates the possibility of forming mixed-ion ordered compounds like previously reported LiK(BH<sub>4</sub>)<sub>2</sub> [76]. For further Li<sup>+</sup> ion kinetic studies, we selected I- and K-substituted LiBH<sub>4</sub>

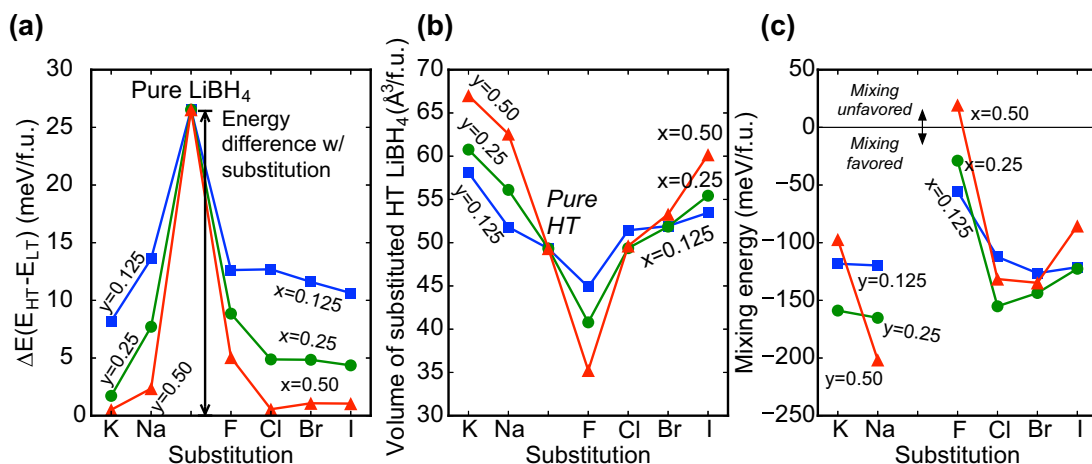


FIG. 1. (a) DFT energy differences between HT- and LT- $\text{LiBH}_4$  phases with and without cation/anion substituents. We tested three different substituent concentrations for each system. (b) Evolution of the DFT volume (per formula unit) in  $(1-x)\text{LiBH}_4 + x\text{LiX}$  and  $(1-y)\text{ABH}_4 + y\text{LiBH}_4$  as a function of the substituents and their concentrations. (c) DFT mixing energy between HT- $\text{LiBH}_4$  and ground-state phases of  $\text{LiX}$  or  $\text{ABH}_4$ .

structures to investigate the effects of halogen and alkali metal substitutions on the transport properties. Previous studies have suggested that the  $\text{Li}^+$  ion conduction is highly dependent on the concentration of substituents in  $\text{LiBH}_4$  [11]; therefore, we simulated two different structures with varying concentrations, namely,  $\text{Li}(\text{BH}_4)_{0.75}\text{I}_{0.25}$  and  $\text{Li}(\text{BH}_4)_{0.5}\text{I}_{0.5}$  compounds. For comparison with the I substitution, we further studied K substitution, as in  $\text{Li}_{0.75}\text{K}_{0.25}\text{BH}_4$ .

#### IV. NATIVE DEFECT CONCENTRATIONS IN HT-LIBH<sub>4</sub>, $\text{Li}(\text{BH}_4)_{1-x}\text{I}_x$ , AND $\text{Li}_{1-y}\text{K}_y\text{BH}_4$

To study the point defects in HT- $\text{LiBH}_4$  and selected systems of  $\text{Li}(\text{BH}_4)_{0.75}\text{X}_{0.25}$ ,  $\text{Li}(\text{BH}_4)_{0.5}\text{X}_{0.5}$ , and  $\text{Li}_{0.75}\text{K}_{0.25}\text{BH}_4$ , we considered the following interstitials with the specified charged states: Li with  $q = +1, 0, -1$ ; H with  $q = +1, 0, -1$ ;  $\text{H}_2$  with  $q = 0$ ; and K with  $q = +1, 0, -1$ . We also examined the following vacancies: Li with  $q = +1, 0, -1$ ; H with  $q = +1, 0, -1$ ; B with  $q = +3, +2, +1, 0, -1, -2, -3$ ;  $\text{BH}_x$  ( $x = 1, 2, 3, 4$ ) with  $q = +1, 0, -1$ ; I with  $q = +1, 0, -1$ ; and K with  $q = +1, 0, -1$ . Additionally, the Li Frenkel defect was also examined. For all these defect types, we evaluated the defect formation energies (Eq. S9) in Ref. [68]) considering

different numbers of geometrical configurations (Table S1 in Ref. [68]).

Here, we only show the formation energies of Li-related defects: defect pair ( $\text{Li}_{\text{Int}}^+, \text{Li}_{\text{Vac}}^-$ ) and Frenkel defect as shown in Fig. 2. We define a defect pair ( $\text{Li}_{\text{Int}}^+, \text{Li}_{\text{Vac}}^-$ ) as the concurrent formation of isolated  $\text{Li}_{\text{Int}}^+$  and  $\text{Li}_{\text{Vac}}^-$ , and the Frenkel defect is the formation of  $\text{Li}_{\text{Int}}^+$  and  $\text{Li}_{\text{Vac}}^-$  which are close with each other. For HT- $\text{LiBH}_4$ , both the Li Frenkel defect and Li defect pair ( $\text{Li}_{\text{Int}}^+, \text{Li}_{\text{Vac}}^-$ ) had negative formation energies:  $-1.3$  and  $-0.9$  eV, respectively ( $0.92$  and  $0.53$  eV, respectively, for LT- $\text{LiBH}_4$ ), which indicates energetically spontaneous Li migrations from their original sites to the nearby interstitial sites. The instability of the compound with respect to Li defects is not unexpected since the HT- $\text{LiBH}_4$  phase is known to be unstable at room temperature [77,78]. For the I- and K-substituted cases, the Li-related formation energies are always positive, which indicates that energy is needed to move the Li ions to interstitial positions. The Li sublattice then becomes stable in these two cases and the substitution stabilization effects are therefore confirmed by defect energies. The dominant Li defect types with the lowest formation energies for  $\text{Li}(\text{BH}_4)_{0.75}\text{I}_{0.25}$ ,  $\text{Li}(\text{BH}_4)_{0.5}\text{I}_{0.5}$ , and  $\text{Li}_{0.75}\text{K}_{0.25}\text{BH}_4$  are the defect pair ( $0.05$  eV), Frenkel

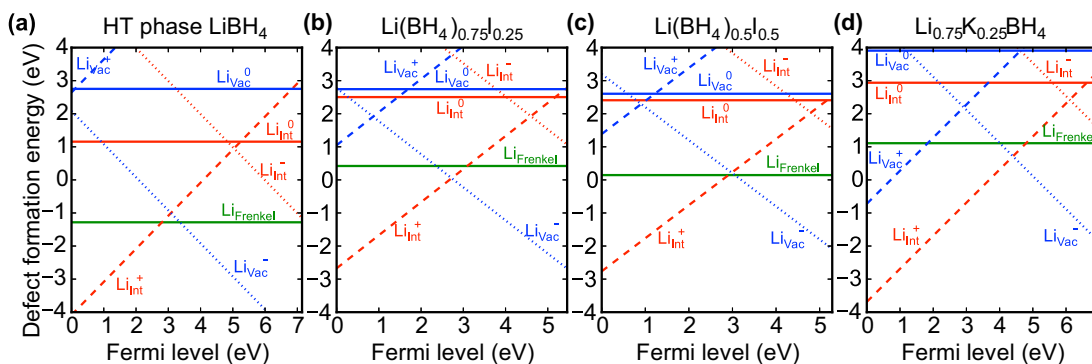


FIG. 2. Calculated formation energies of Li-related defects in (a) HT- $\text{LiBH}_4$ , (b)  $\text{Li}(\text{BH}_4)_{0.75}\text{I}_{0.25}$ , (c)  $\text{Li}(\text{BH}_4)_{0.5}\text{I}_{0.5}$ , and (d)  $\text{Li}_{0.75}\text{K}_{0.25}\text{BH}_4$  as a function of Fermi energy with respect to the valence-band maximum.

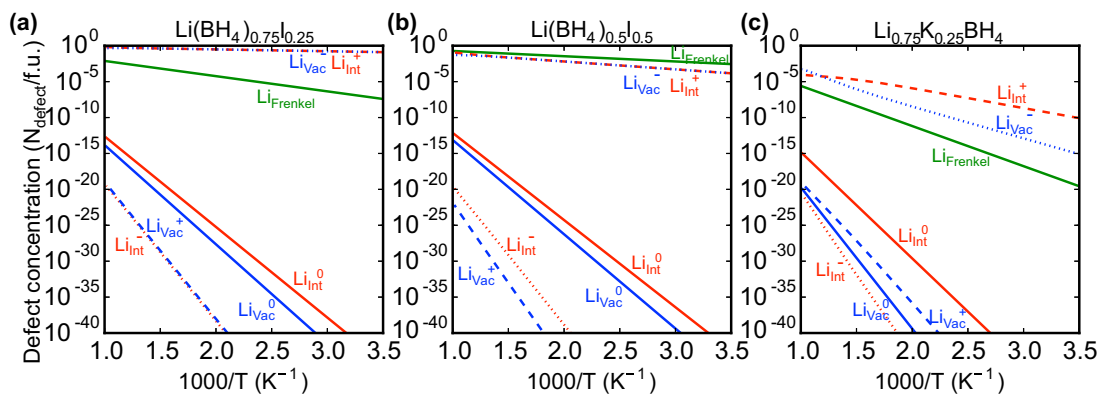


FIG. 3. Li-related defect concentrations in (a)  $\text{Li}(\text{BH}_4)_{0.75}\text{I}_{0.25}$ , (b)  $\text{Li}(\text{BH}_4)_{0.5}\text{I}_{0.5}$ , and (c)  $\text{Li}_{0.75}\text{K}_{0.25}\text{BH}_4$  as a function of temperature. The highest defect concentrations at room temperature for these three cases were  $10^{-1}$ ,  $10^{-3}$ , and  $10^{-10}$  per formula unit, respectively.

defect (0.15 eV), and defect pair (0.44 eV), respectively. It is noteworthy that the Frenkel defect is more favorable in  $\text{Li}(\text{BH}_4)_{0.5}\text{I}_{0.5}$  compared with the formation of individual Li interstitials and vacancies. With increasing  $\text{I}^-$  concentration from  $x = 0.25$  to 0.50, the dominant defect formation energy increased from 0.05 to 0.15 eV, whereas the bulk energy difference ( $\Delta E$ ) between HT and LT phases decreased from 48 to 11 meV per formula unit. We therefore conclude from Fig. 2 that enhanced stabilization is associated with the increase of the defect formation energies; however, this behavior of defect energies can decrease the total defect concentration in the system and therefore impairs its ionic conductivity as discussed below.

The calculated temperature-dependent native defect concentrations in  $\text{Li}(\text{BH}_4)_{0.75}\text{I}_{0.25}$ ,  $\text{Li}(\text{BH}_4)_{0.5}\text{I}_{0.5}$ , and  $\text{Li}_{0.75}\text{K}_{0.25}\text{BH}_4$ , which were calculated by solving equations S8–S10, are presented in Fig. 3. The calculation of defect concentrations is problematic for HT- $\text{LiBH}_4$  because of its negative defect formation energy. As previously mentioned,

the defect formation energy increase caused by the structural stabilization with cation/anion substitutions decrease the room-temperature Li-related defect concentrations. The concentrations of dominant defects at room temperature for these three cases [ $\text{Li}(\text{BH}_4)_{0.75}\text{I}_{0.25}$ ,  $\text{Li}(\text{BH}_4)_{0.5}\text{I}_{0.5}$ , and  $\text{Li}_{0.75}\text{K}_{0.25}\text{BH}_4$ ] were  $10^{-1}$ ,  $10^{-3}$ , and  $10^{-10}$  per formula unit, as observed in Fig. 3.

## V. LITHIUM ION MASS TRANSPORT IN $\text{Li}(\text{BH}_4)_{1-x}\text{I}_x$ AND $\text{Li}_{1-y}\text{K}_y\text{BH}_4$

In this section, we present the lithium ion conductivities calculated for the  $\text{Li}(\text{BH}_4)_{0.75}\text{I}_{0.25}$ ,  $\text{Li}(\text{BH}_4)_{0.5}\text{I}_{0.5}$ , and  $\text{Li}_{0.75}\text{K}_{0.25}\text{BH}_4$  systems using a combination of the NEB method and KMC simulations. Spatial lithium ion diffusion networks of both interstitials and vacancies were built for all these cases based on all of the interstitial and vacancy sites, as demonstrated in Fig. 4. Different numbers of diffusion pathways were considered for the interstitials and vacancies,

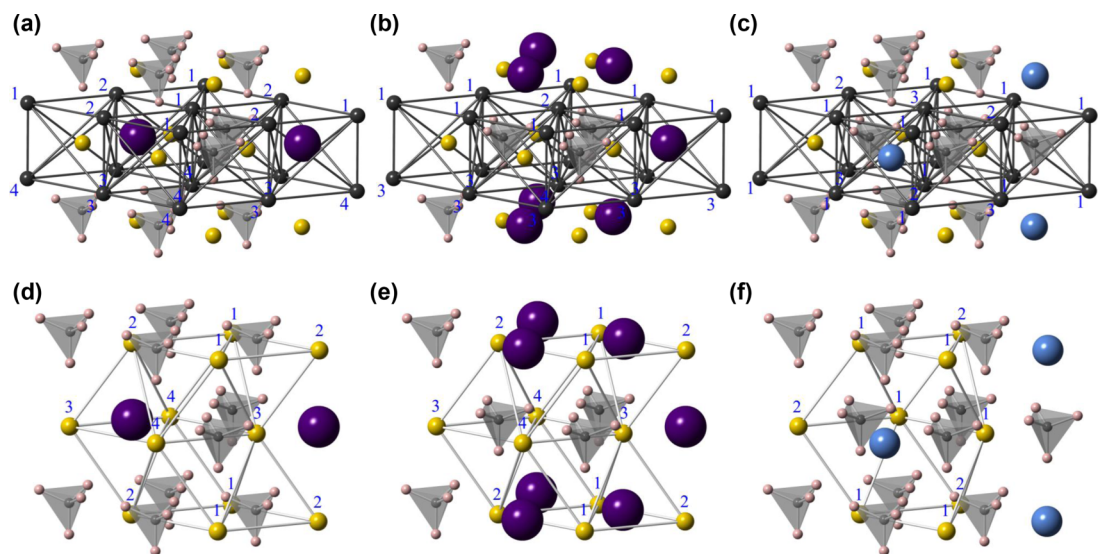


FIG. 4. Lithium-ion defect diffusion network: interstitial paths in (a)  $\text{Li}(\text{BH}_4)_{0.75}\text{I}_{0.25}$ , (b)  $\text{Li}(\text{BH}_4)_{0.5}\text{I}_{0.5}$ , and (c)  $\text{Li}_{0.75}\text{K}_{0.25}\text{BH}_4$  and vacancy paths in (d)  $\text{Li}(\text{BH}_4)_{0.75}\text{I}_{0.25}$ , (e)  $\text{Li}(\text{BH}_4)_{0.5}\text{I}_{0.5}$ , and (f)  $\text{Li}_{0.75}\text{K}_{0.25}\text{BH}_4$ . The black (silver) lines represent the interstitial (vacancy) lithium-ion diffusion paths between different defect sites (the numbers in blue). The gold, black, blue, dark grey, light grey, and violet circles represent Li (and vacancy sites), Li interstitial sites, K, B, H, and I, respectively.

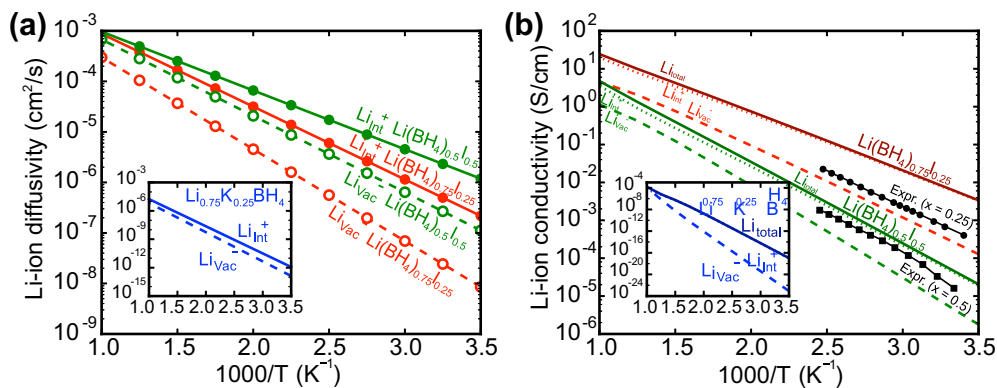


FIG. 5. (a) Calculated lithium-ion defect diffusivities of  $\text{Li}(\text{BH}_4)_{0.75}\text{I}_{0.25}$ ,  $\text{Li}(\text{BH}_4)_{0.5}\text{I}_{0.5}$ , and  $\text{Li}_{0.75}\text{K}_{0.25}\text{BH}_4$  as a function of temperature. (b) Calculated lithium-ion defect conductivities of  $\text{Li}(\text{BH}_4)_{0.75}\text{I}_{0.25}$ ,  $\text{Li}(\text{BH}_4)_{0.5}\text{I}_{0.5}$ , and  $\text{Li}_{0.75}\text{K}_{0.25}\text{BH}_4$  as a function of temperature (attempt frequency  $\nu = 10^{13}$ ). The experimental conductivity profiles were adopted from Refs. [11,38].

and the subsequent energy barriers were examined for all these pathways (see Table S2 in Ref. [68]).

We report the lowest barriers of 0.14 and 0.25 eV for interstitial and vacancy diffusion, respectively, in  $\text{Li}(\text{BH}_4)_{0.75}\text{I}_{0.25}$ , which is consistent with previous work [39]. In the  $\text{Li}(\text{BH}_4)_{0.5}\text{I}_{0.5}$  system, very similar preferred paths were identified for interstitial and vacancy diffusion with the lowest barriers of 0.20 and 0.18 eV, respectively. In  $\text{Li}_{0.75}\text{K}_{0.25}\text{BH}_4$ , both interstitial and vacancy diffusion were observed to be difficult, with the lowest barriers of 0.56 and 0.59 eV, respectively. The KMC simulations were also performed at a series of temperatures for each type of defect using all the energy barriers obtained. The diffusivity pre-factor  $D_0$  and  $Q$  were fitted, and all the diffusivity profiles as a function of temperature are presented in Fig. 5(a).

At room temperature, the lithium-ion diffusivities in  $\text{Li}(\text{BH}_4)_{0.75}\text{I}_{0.25}$  were  $10^{-7}$   $\text{cm}^2/\text{s}$  (interstitial mechanism) and  $10^{-8}$   $\text{cm}^2/\text{s}$  (vacancy mechanism). The corresponding lithium-ion diffusivities in  $\text{Li}(\text{BH}_4)_{0.5}\text{I}_{0.5}$  were  $\sim 10^{-6}$  and  $10^{-7}$   $\text{cm}^2/\text{s}$ , respectively. For  $\text{Li}_{0.75}\text{K}_{0.25}\text{BH}_4$ , the lithium-ion diffusion at room temperature has a calculated diffusivity of  $10^{-12}$   $\text{cm}^2/\text{s}$ , not fast enough for SSE applications. Overall, interstitial diffusion is preferred in all the systems, which is speculated to be the result of the volume expansion and thus enlarged interstitial diffusion channels caused by the I- or K-substitutions in  $\text{LiBH}_4$ .

In addition, the conductivities in Fig. 5(b) were calculated using Eq. (S6) in Ref. [68] and the defect diffusivities and concentrations previously obtained (by adding the interstitial and vacancy conductivities). The computed conductivity profiles of  $\text{Li}(\text{BH}_4)_{1-x}\text{I}_x$  ( $x = 0.25, 0.5$ ) in Fig. 5(b) demonstrate the reasonable agreement with the experimental observations. The overestimation is reasonable, as we performed the simulations within a perfect crystal structure (i.e., without any impurities or grain boundaries), which can further lead to a decreased experimental  $\text{Li}^+$  ion conductivity [79]. The conductivity profile of  $\text{Li}(\text{BH}_4)_{0.75}\text{I}_{0.25}$  is much higher than that of its  $\text{Li}(\text{BH}_4)_{0.5}\text{I}_{0.5}$  counterpart with a larger room-temperature conductivity of  $5.7 \times 10^{-3}$  S/cm (compared with  $4.2 \times 10^{-5}$  S/cm for  $\text{Li}(\text{BH}_4)_{0.5}\text{I}_{0.5}$ ). It is noteworthy that the trend of the diffusivity profiles was opposite to that of the conductivity, with easier lithium ion migration observed for

the  $\text{Li}(\text{BH}_4)_{0.5}\text{I}_{0.5}$  system in Fig. 5(a). The higher lithium ion conductivity in  $\text{Li}(\text{BH}_4)_{0.75}\text{I}_{0.25}$  can be attributed to its higher defect concentration because of the lower defect formation energies and decreased stabilization effects. Therefore the experimentally observed fluctuations in the conductivity profile versus concentration [11,38,80] of  $\text{Li}(\text{BH}_4)_{1-x}\text{I}_x$  systems can be explained by the competing effects between the defect concentration and  $\text{Li}^+$  ion mobility caused by the substitutional effects. We conclude that the stabilization of HT- $\text{LiBH}_4$  should be carefully tuned to permit the formation of a sufficient amount of defects to facilitate fast lithium ion conduction.

## VI. CONCLUSION

In this work, we showed that various cation/anion substitutional effects in HT- $\text{LiBH}_4$  (i.e., halogen substitution of F, Cl, Br, and I at the  $\text{BH}_4$  site and alkali metal substitution of Na and K at the Li site) decrease the ground-state energy difference between the HT phase and the stable ground-state LT phase. We observed that it was most effective to substitute  $\text{I}^-$  for  $\text{BH}_4$  or  $\text{K}^+$  for  $\text{Li}^+$  to achieve the stabilization of the HT phase at an equal substituent concentration. A positive relation between the substituent concentration and energetic stabilization of the HT phase was found. The moderately sized ions ( $\text{Br}^-$ ,  $\text{I}^-$ , and  $\text{Na}^+$ ) lead to a lower mixing energy compared with the substituents with larger ionic radii (e.g.,  $\text{K}^+$ ,  $\text{I}^-$ ) or smaller ionic radii (e.g.,  $\text{F}^-$ ). The calculated mixing energies of HT- $\text{LiBH}_4$  and  $\text{LiX}$  or  $\text{ABH}_4$  were negative (except  $\text{F}^-$ ), which are consistent with the experimentally observed solid-solution formation for a wide range of substituent concentrations. The stabilization of HT- $\text{LiBH}_4$  increased the defect formation energy, leading to a lower defect concentration. In  $\text{Li}(\text{BH}_4)_{1-x}\text{I}_x$ , we observed that a higher  $\text{I}^-$  concentration yielded a higher diffusivity but with a lower conductivity. The nonmonotonic relation between the concentration and conductivity is a result of competing effects between the diffusivity and defect concentration. The lithium ion conductivity obtained by K substitution at the Li site was observed to be very low because of the blocking of the lithium ion diffusion pathway by K ions and the narrow diffusion channel. We emphasize that the stabilization of a  $\text{LiBH}_4$ -based lithium ion conductor can be experimentally optimized by careful selection of cation/anion substituents

and their concentrations, which can further realize the highest lithium ion conduction in  $\text{LiBH}_4$ .

#### ACKNOWLEDGMENTS

Z.Y. and C.W. (DFT stability, defect formation energy, and conductivity) acknowledge supports from the Center for Electrochemical Energy Science (CEES), an Energy Frontier Research Center funded by the US Department of Energy, Office of Science, Basic Energy Sciences under Award No. DEAC02-06CH11357. S.K. (initial defect calculations) was supported by the financial assistance Award No. 70NANB14H012 from

U.S. Department of Commerce, National Institute of Standards and Technology as part of the Center for Hierarchical Materials Design (CHiMaD). K.M. (KMC simulations) acknowledges the support from the US Department of Energy, Office of Science, Basic Energy Sciences, under Grant No. DEFG02-07ER46433. M.A. (structure analysis) was supported by the Dow Chemical Company. We gratefully acknowledge the computing resources from (1) the National Energy Research Scientific Computing Center, a DOE Office of Science User Facility supported under Contract No. DE-AC02-05CH11231 and (2) Blues, a high-performance computing cluster operated by the Laboratory Computing Resource Center at Argonne National Laboratory.

- 
- [1] J. B. Goodenough, *Energy Environ. Sci.* **7**, 14 (2014).  
 [2] K. Ozawa, *Solid State Ionics* **69**, 212 (1994).  
 [3] J. M. Tarascon and M. Armand, *Nature (London)* **414**, 359 (2001).  
 [4] J. B. Goodenough and Y. Kim, *Chem. Mater.* **22**, 587 (2010).  
 [5] P. Arora, R. E. White, and M. Doyle, *J. Electrochem. Soc.* **145**, 3647 (1998).  
 [6] D. H. Jang, Y. J. Shin, and S. M. Oh, *J. Electrochem. Soc.* **143**, 2204 (1996).  
 [7] J. C. Bachman, S. Muy, A. Grimaud, H.-H. Chang, N. Pour, S. F. Lux, O. Paschos, F. Maglia, S. Lupart, P. Lamp, L. Giordano, and Y. Shao-Horn, *Chem. Rev.* **116**, 140 (2016).  
 [8] A. Rabenau, *Solid State Ionics* **6**, 277 (1982).  
 [9] H. Maekawa, M. Matsuo, H. Takamura, M. Ando, Y. Noda, T. Karahashi, and S. Orimo, *J. Am. Chem. Soc.* **131**, 894 (2009).  
 [10] M. Matsuo, H. Takamura, H. Maekawa, H.-W. Li, and S. Orimo, *Appl. Phys. Lett.* **94**, 084103 (2009).  
 [11] D. Sveinbjörnsson, J. S. G. Myrdal, D. Blanchard, J. J. Bentzen, T. Hirata, M. B. Mogensen, P. Norby, S.-I. Orimo, and T. Vegge, *J. Phys. Chem. C* **117**, 3249 (2013).  
 [12] M. B. Ley, D. B. Ravnsbæk, Y. Filinchuk, Y.-S. Lee, R. Janot, Y. W. Cho, J. Skibsted, and T. R. Jensen, *Chem. Mater.* **24**, 1654 (2012).  
 [13] M. B. Ley, S. Boulineau, R. Janot, Y. Filinchuk, and T. R. Jensen, *J. Phys. Chem. C* **116**, 21267 (2012).  
 [14] Y. Yan, R.-S. Kühnel, A. Remhof, L. Duchêne, E. C. Reyes, D. Rentsch, Z. Łodziana, and C. Battaglia, *Adv. Energy Mater.* **7**, 1700294 (2017).  
 [15] Y. Inaguma, C. Liqun, M. Itoh, T. Nakamura, T. Uchida, H. Ikuta, and M. Wakihara, *Solid State Commun.* **86**, 689 (1993).  
 [16] H.-J. Deiseroth, S.-T. Kong, H. Eckert, J. Vannahme, C. Reiner, T. Zaiß, and M. Schlosser, *Angew. Chemie Int. Ed.* **47**, 755 (2008).  
 [17] V. Thangadurai, J. Schwenzel, and W. Weppner, *Ionics (Kiel)* **11**, 11 (2005).  
 [18] K. Arbi, J. M. Rojo, and J. Sanz, *J. Eur. Ceram. Soc.* **27**, 4215 (2007).  
 [19] P. G. Bruce, *J. Electrochem. Soc.* **130**, 662 (1983).  
 [20] N. Kamaya, K. Homma, Y. Yamakawa, M. Hirayama, R. Kanno, M. Yonemura, T. Kamiyama, Y. Kato, S. Hama, K. Kawamoto, and A. Mitsui, *Nat. Mater.* **10**, 682 (2011).  
 [21] S. P. Ong, Y. Mo, W. D. Richards, L. Miara, H. S. Lee, and G. Ceder, *Energy Environ. Sci.* **6**, 148 (2013).  
 [22] M. Matsuo and S. Orimo, *Adv. Energy Mater.* **1**, 161 (2011).  
 [23] A. Züttel, P. Wenger, S. Rentsch, P. Sudan, P. Mauron, and C. Emmenegger, *J. Power Sources* **118**, 1 (2003).  
 [24] A. Züttel, S. Rentsch, P. Fischer, P. Wenger, P. Sudan, P. Mauron, and C. Emmenegger, *J. Alloys Compd.* **356-357**, 515 (2003).  
 [25] Y. Zhang, Y. Wang, K. Michel, and C. Wolverton, *Phys. Rev. B* **86**, 094111 (2012).  
 [26] M. Matsuo, Y. Nakamori, S. Orimo, H. Maekawa, and H. Takamura, *Appl. Phys. Lett.* **91**, 224103 (2007).  
 [27] E. Orgaz, A. Membrillo, R. Castañeda, and A. Aburto, *J. Alloys Compd.* **404-406**, 176 (2005).  
 [28] M. H. W. Verkuijlen, P. Ngene, D. W. de Kort, C. Barré, A. Nale, E. R. H. van Eck, P. J. M. van Bentum, P. E. de Jongh, and A. P. M. Kentgens, *J. Phys. Chem. C* **116**, 22169 (2012).  
 [29] D. Blanchard, A. Nale, D. Sveinbjörnsson, T. M. Eggenhuisen, M. H. W. Verkuijlen, T. Vegge, A. P. M. Kentgens, and P. E. de Jongh, *Adv. Funct. Mater.* **25**, 184 (2015).  
 [30] S. Das, P. Ngene, P. Norby, T. Vegge, P. E. de Jongh, and D. Blanchard, *J. Electrochem. Soc.* **163**, A2029 (2016).  
 [31] L. Mosegaard, B. Moller, J.-E. Jørgensen, Y. Filinchuk, Y. Cerenius, J. C. Hanson, E. Dimasi, F. Besenbacher, and T. R. Jensen, *J. Phys. Chem. C* **112**, 1299 (2008).  
 [32] L. H. Rude, O. Zavorotyńska, L. M. Arnbjerg, D. B. Ravnsbæk, R. A. Malmkjær, H. Grove, B. C. Hauback, M. Baricco, Y. Filinchuk, F. Besenbacher, and T. R. Jensen, *Int. J. Hydrogen Energy* **36**, 15664 (2011).  
 [33] L. M. Arnbjerg, D. B. Ravnsbæk, Y. Filinchuk, R. T. Vang, Y. Cerenius, F. Besenbacher, J.-E. Jørgensen, H. J. Jakobsen, and T. R. Jensen, *Chem. Mater.* **21**, 5772 (2009).  
 [34] A. Borgschulte, R. Gremaud, S. Kato, N. P. Stadie, A. Remhof, A. Züttel, M. Matsuo, and S.-I. Orimo, *Appl. Phys. Lett.* **97**, 031916 (2010).  
 [35] L. H. Rude, E. Groppo, L. M. Arnbjerg, D. B. Ravnsbæk, R. A. Malmkjær, Y. Filinchuk, M. Baricco, F. Besenbacher, and T. R. Jensen, *J. Alloys Compd.* **509**, 8299 (2011).  
 [36] P. E. de Jongh, D. Blanchard, M. Matsuo, T. J. Udovic, and S. Orimo, *Appl. Phys. A* **122**, 251 (2016).  
 [37] H. Oguchi, M. Matsuo, J. S. Hummelshøj, T. Vegge, J. K. Nørskov, T. Sato, Y. Miura, H. Takamura, H. Maekawa, and S. Orimo, *Appl. Phys. Lett.* **94**, 141912 (2009).  
 [38] R. Miyazaki, T. Karahashi, N. Kumatani, Y. Noda, M. Ando, H. Takamura, M. Matsuo, S. Orimo, and H. Maekawa, *Solid State Ionics* **192**, 143 (2011).

- [39] J. S. G. Myrdal, D. Blanchard, D. Sveinbjörnsson, and T. Vegge, *J. Phys. Chem. C* **117**, 9084 (2013).
- [40] J. S. G. Myrdal, D. Sveinbjörnsson, and T. Vegge, in *ECS Meeting Abstracts*, MA2011-02, 756 (2011).
- [41] N. Bernstein, M. D. Johannes, and K. Hoang, *Phys. Rev. B* **88**, 220102 (2013).
- [42] A. Van der Ven, M. K. Aydinol, G. Ceder, G. Kresse, and J. Hafner, *Phys. Rev. B* **58**, 2975 (1998).
- [43] G. Ceder, Y.-M. Chiang, D. R. Sadoway, M. K. Aydinol, Y.-I. Jang, and B. Huang, *Nature* **392**, 694 (1998).
- [44] D. Morgan, A. Van der Ven, and G. Ceder, *Electrochem. Solid-State Lett.* **7**, A30 (2004).
- [45] K. Kang, Y. S. Meng, J. Bréger, C. P. Grey, G. Ceder, and G. Ceder, *Science* **311**, 977 (2006).
- [46] M. M. Thackeray, C. Wolverton, and E. D. Isaacs, *Energy Environ. Sci.* **5**, 7854 (2012).
- [47] Y. S. Meng and M. E. Arroyo-de Dompablo, *Energy Environ. Sci.* **2**, 589 (2009).
- [48] S. Kim, M. Aykol, and C. Wolverton, *Phys. Rev. B* **92**, 115411 (2015).
- [49] L. Jaber-Ansari, K. P. Puntambekar, S. Kim, M. Aykol, L. Luo, J. Wu, B. D. Myers, H. Iddir, J. T. Russell, S. J. Saldaña, R. Kumar, M. M. Thackeray, L. A. Curtiss, V. P. Dravid, C. Wolverton, and M. C. Hersam, *Adv. Energy Mater.* **5**, 1500646 (2015).
- [50] M. Aykol, S. Kim, and C. Wolverton, *J. Phys. Chem. C* **119**, 19053 (2015).
- [51] J.-H. Cho, M. Aykol, S. Kim, J.-H. Ha, C. Wolverton, K. Y. Chung, K.-B. Kim, and B.-W. Cho, *J. Am. Chem. Soc.* **136**, 16116 (2014).
- [52] M. Aykol, S. Kirklin, and C. Wolverton, *Adv. Energy Mater.* **4**, 1400690 (2014).
- [53] M. Amsler, Z. Yao, and C. Wolverton, *Chem. Mater.* **29**, 9819 (2017).
- [54] H. Bin, Z. Yao, S. Zhu, C. Zhu, H. Pan, Z. Chen, C. Wolverton, and D. Zhang, *J. Alloys Compd.* **695**, 1223 (2017).
- [55] Q. Li, H. Liu, Z. Yao, J. Cheng, T. Li, Y. Li, C. Wolverton, J. Wu, and V. P. Dravid, *ACS Nano* **10**, 8788 (2016).
- [56] C. Zhan, Z. Yao, J. Lu, L. Ma, V. A. Maroni, L. Li, E. Lee, E. E. Alp, T. Wu, J. Wen, Y. Ren, C. Johnson, M. M. Thackeray, M. K. Y. Chan, C. Wolverton, and K. Amine, *Nat. Energy* **2**, 963 (2017).
- [57] Z. Yao, S. Kim, M. Aykol, Q. Li, J. Wu, J. He, and C. Wolverton, *Chem. Mater.* **29**, 9011 (2017).
- [58] Z. Yao, S. Kim, J. He, V. I. Hegde, and C. Wolverton, *Sci. Adv.* **4**, eaao6754 (2018).
- [59] S. Hwang, Z. Yao, L. Zhang, M. Fu, K. He, L. Mai, C. Wolverton, and D. Su, *ACS Nano* **12**, 3638 (2018).
- [60] K. He, Z. Yao, S. Hwang, N. Li, K. Sun, H. Gan, Y. Du, H. Zhang, C. Wolverton, and D. Su, *Nano Lett.* **17**, 5726 (2017).
- [61] G. Kresse and J. Furthmüller, *Phys. Rev. B* **54**, 11169 (1996).
- [62] J. P. Perdew and Y. Wang, *Phys. Rev. B* **45**, 13244 (1992).
- [63] P. E. Blöchl, *Phys. Rev. B* **50**, 17953 (1994).
- [64] C. Wolverton and V. Ozoliņš, *Phys. Rev. B* **75**, 064101 (2007).
- [65] K. J. Michel, Y. Zhang, and C. Wolverton, *J. Phys. Chem. C* **117**, 19295 (2013).
- [66] G. L. W. Hart and R. W. Forcade, *Phys. Rev. B* **77**, 224115 (2008).
- [67] Q. Li, J. Wu, Z. Yao, M. M. Thackeray, C. Wolverton, and V. P. Dravid, *Nano Energy* **44**, 15 (2017).
- [68] See Supplemental Material at <http://link.aps.org/supplemental/10.1103/PhysRevMaterials.2.065402> for the methodology details on mixing energy, chemical potential, defect conductivity calculations and the full set of defect configurations and barriers.
- [69] G. Henkelman and H. Jónsson, *J. Chem. Phys.* **113**, 9978 (2000).
- [70] G. Henkelman, B. P. Uberuaga, and H. Jónsson, *J. Chem. Phys.* **113**, 9901 (2000).
- [71] K. J. Michel and C. Wolverton, *Comput. Phys. Commun.* **185**, 1389 (2014).
- [72] L. Ward and K. Michel, materials/mint: Initial Release (2016), <https://doi.org/10.5281/zenodo.167890>.
- [73] R. D. Shannon and IUCr, *Acta Crystallogr. Sect. A* **32**, 751 (1976).
- [74] J. S. Hummelshøj, D. D. Landis, J. Voss, T. Jiang, A. Tekin, N. Bork, M. Duřak, J. J. Mortensen, L. Adamska, J. Andersin, J. D. Baran, G. D. Barmparis, F. Bell, A. L. Bezanilla, J. Bjork, M. E. Björketun, F. Bleken, F. Buchter, M. Bürkle, P. D. Burton, B. B. Buus, A. Calborean, F. Calle-Vallejo, S. Casolo, B. D. Chandler, D. H. Chi, I. Czekaj, S. Datta, A. Datye, A. DeLaRiva, V. Despoja, S. Dobrin, M. Engelund, L. Ferrighi, P. Frondelius, Q. Fu, A. Fuentes, J. Fürst, A. García-Fuente, J. Gavnholt, R. Goeke, S. Gudmundsdóttir, K. D. Hammond, H. A. Hansen, D. Hibbitts, E. Hobi, J. G. Howalt, S. L. Hruby, A. Huth, L. Isaeva, J. Jelic, I. J. T. Jensen, K. A. Kacprzak, A. Kelkkanen, D. Kelsey, D. S. Kesanakurthi, J. Kleis, P. J. Klüpfel, I. Konstantinov, R. Korytar, P. Koskinen, C. Krishna, E. Kunkes, A. H. Larsen, J. M. G. Lastra, H. Lin, O. Lopez-Acevedo, M. Mantega, J. I. Martínez, I. N. Mesa, D. J. Mowbray, J. S. G. Mýrdal, Y. Natanzon, A. Nistor, T. Olsen, H. Park, L. S. Pedroza, V. Petzold, C. Plaisance, J. A. Rasmussen, H. Ren, M. Rizzi, A. S. Ronco, C. Rostgaard, S. Saadi, L. A. Salguero, E. J. G. Santos, A. L. Schoenhalz, J. Shen, M. Smedemand, O. J. Stausholm-Møller, M. Stibius, M. Strange, H. B. Su, B. Temel, A. Toftelund, V. Tripkovic, M. Vanin, V. Viswanathan, A. Vojvodic, S. Wang, J. Wellendorff, K. S. Thygesen, J. Rossmeisl, T. Bligaard, K. W. Jacobsen, J. K. Nørskov, and T. Vegge, *J. Chem. Phys.* **131**, 014101 (2009).
- [75] O. Zavorotynska, M. Corno, E. Pinatel, L. H. Rude, P. Ugliengo, T. R. Jensen, and M. Baricco, *Crystals* **2**, 144 (2012).
- [76] E. A. Nickels, M. O. Jones, W. I. F. David, S. R. Johnson, R. L. Lowton, M. Sommariva, and P. P. Edwards, *Angew. Chemie Int. Ed.* **47**, 2817 (2008).
- [77] K. Hoang and C. G. Van de Walle, *Int. J. Hydrogen Energy* **37**, 5825 (2012).
- [78] Z. Łodziana and T. Vegge, *Phys. Rev. Lett.* **93**, 145501 (2004).
- [79] M. Park, X. Zhang, M. Chung, G. B. Less, and A. M. Sastry, *J. Power Sources* **195**, 7904 (2010).
- [80] A. V. Skripov, A. V. Soloninin, M. B. Ley, T. R. Jensen, and Y. Filinchuk, *J. Phys. Chem. C* **117**, 14965 (2013).